The Beginning of Sediment Transport – A Different Approach

R. Aleixo & R. Maia
Departamento de Engenharia Civil, Faculdade de Engenharia da Universidade do Porto
Rua Dr. Roberto Frias s/n, 4200-465 Porto, Portugal

ABSTRACT: The beginning of motion of particles at the bottom of a water channel is a result of a rather complex interaction between the flow and the particles. Using a simplified bed model it is possible to easily study and isolate the interactions between the flow and the bed and to better define the conditions leading to the beginning of bed particles motion. A theoretical approach that takes into account the different parameters such as support angle and turbulence intensity, is presented and compared with the Shields diagram and experimental results. This study is the first phase of a broader research project in course who aims to better understand and explain the beginning of sediment particles motion.

1 INTRODUCTION

Aiming to study the interaction between the flow and the channel bed, a simple model was developed in order to allow a proper description of that interaction in terms of its physics. Some assumptions were made and based on the known results of the boundary layer theory.

This work summarizes the first stage of a broader research project in course at the Hydraulics Laboratory of Faculty of Engineering of Porto University, currently focused at the study of the flow around a single particle, aiming to be used in future work to characterize the interaction between particles.

2 CONCEPTUAL MODEL

The bed model studied consists on a flat and horizontal plate in which a localized two-particles' width bed, with the full transverse length of the water channel was provided, as depicted in Figure 1. Over this bed of particles, at the channel axis, a single particle was placed. The particles that support that single particle will be from now on referred as supporting particles and the single particle will be designated as test-particle. This model consists in a simplification of one presented by (Nezu and Nakagawa 1993).

There are two possible 3D configurations to support the test-particle: a three- or a four-particles bed arrangement. For this analysis the test-particle is assumed to be supported by a four particles bed arrangement with the centres of the five spheres forming a square-based pyramid as shown in Figure 2. It can be shown that the maximum height of the sphere is $h_{1t} = d/\sqrt{2}$ and that the support angle is $\theta = \text{atan}\sqrt{2}/2 = 35.26^{\text{o}}$ (as depicted on Fig 2).

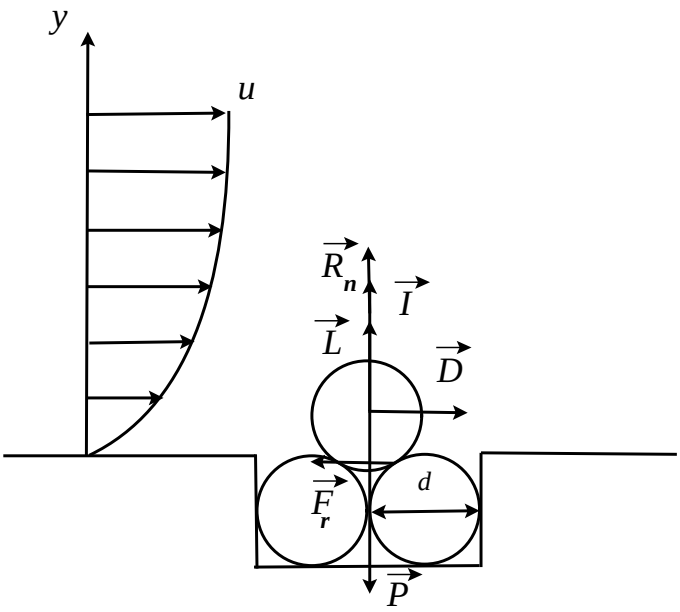

Figure 1: Simplified bed model. A test-particle, with the same diameter as the ones of the bed is immersed on a flow with a velocity profile $u = u(y)$. The forces acting on a particle (referred as test-particle) are the weight $\vec{P}$, the drag $\vec{D}$, the lift $\vec{L}$, the buoyancy $\vec{I}$, the normal reaction $\vec{R_n}$, the friction force $\vec{F_r}$, and d is the particle's diameter.

For this simple model theoretical hypothesis regarding the beginning of motion were assumed:

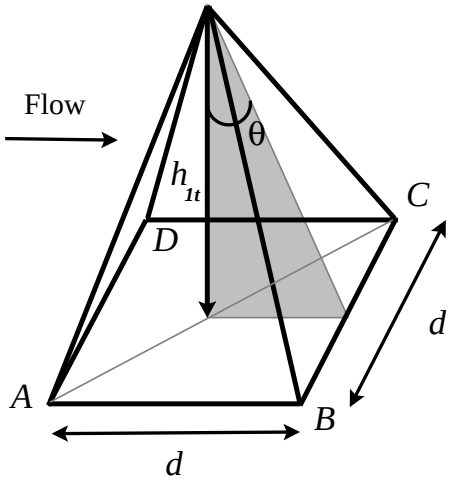

Figure 2: A squared based pyramid results from the four-spheres support arrangement considered in this study, being θ the supporting angle. Flow direction is perpendicular to the segment AD.

1. the flow is processed over a flat smooth bed until it reaches the test-particle.
2. the flow is bidimensional and developed, so that the longitudinal component, u, is much larger than the vertical and transversal components v and w, respectively;
3. the boundary-layer is limited to a narrow region near the bed, so that the test-particle may be considered, in this approach, immersed in a uniform stream, of velocity U_∞;
4. outside the boundary layer, the turbulence intensity profile will be assumed constant (Hinze 1975);
5. the flow is fully established;

2.1 Analysis of the Forces Acting on the Test-Particle

The forces acting on the test-particle are the following (considering an horizontal plate) are:

- The immersed weight force, $\vec{P} - \vec{I}$:

$$P - I = \frac{\pi}{6}(\rho_s - \rho)gd^3 \tag{1}$$

where ρ_s = density of the particle; ρ = density of the water; g = acceleration of gravity; and d = particle's diameter.

- The drag, $\vec{D}$, and lift, $\vec{L}$, forces (Goldstein 1965):

$$D = \frac{1}{2}\rho U_\infty^2 S C_D \tag{2}$$

$$L = \frac{1}{2}\rho U_\infty^2 S C_L \tag{3}$$

where U_∞ = velocity of the flow far from the bed; S =particle's section exposed to the flow; C_D = the drag coefficient; and C_L = lift coefficient.

- The resistance force, $\vec{F_r}$ which can be expressed as (Halliday et al. 2001):

$$F_r = \mu_e R_n \tag{4}$$

where μ_e = static friction coefficient; and R_n = normal reaction.

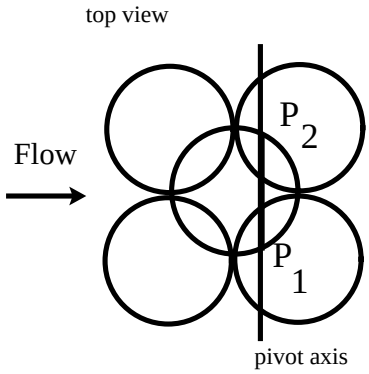

Figure 3: Top view of the particle arrangement and representation of the pivot points (P_1 and P_2) and axis formed by those points. Flow direction is perpendicular to the segment P_1P_2.

From the equilibrium conditions, $\sum \vec{F} = 0$ and $\sum \vec{M} = 0$, where $\vec{F}$ represents the resultant force and $\vec{M}$ the resulting torque, one obtains respectively for the force balance:

$$\frac{U_\infty^2}{(s-1)gd} = \frac{4}{3C_D}\left(\frac{\mu_e}{1 + \dfrac{C_L}{C_D}\mu_e}\right) \tag{5}$$

and for the torque balance:

$$\frac{U_\infty^2}{(s-1)gd} = \frac{4}{3C_D}\left(\frac{\tan\theta}{1 + \dfrac{C_L}{C_D}\tan\theta}\right) \tag{6}$$

where θ = support angle, as represented in Figure 2; and $s = \rho_s/\rho$. According to observations for the studied case conditions and considering current values of static friction coefficients for glass and *perspex* (0.7 to 0.9), equation (6) was taken as the critical reference in the following analysis.

The first member of equation (6) can be identified as a Froude number, and so the following relation can be written:

$$\mathrm{Fr} = f(C_D, C_L, \theta, \phi) \tag{7}$$

where C_D and C_L are functions of the particle Reynolds number, defined as $\mathrm{Re}_p = U_\infty d/\nu$ and of the shear rate defined as $\partial u/\partial y$ (Saffman 1964). For C_D and C_L, formulations corresponding to the situation of a sphere in a shear flow should be used, if available.

In accordance with the model's theoretical hypothesis referred (as 3.) before, it was assumed that C_L was zero (Goldstein 1965), corresponding to, on a first approach, not taking into account lift force effects. That simplification was assumed although having in mind that, accordingly to (Saffman 1964), a sphere in a slow shear flow is submitted to a lift force. Therefore equation (6) can be written:

$$\frac{U_\infty^2}{(s-1)gd} = \frac{4}{3C_D}\tan\theta \tag{8}$$

or, multiplying both terms by the squared shear velocity, $u_*^2 = \tau_w/\rho$:

$$\frac{u_*^2}{(s-1)gd} = \frac{4}{3U_\infty^{+2}C_D}\tan\theta \tag{9}$$

where $U_\infty^+ = U_\infty/u_*$. For turbulent boundary layer flows, and using the skin friction coefficient definition, it is possible to demonstrate that $u_*/U_\infty \approx 1/20$. The left hand side of equation (9) may be identified as the Shields parameter (Shields 1936) and will be denoted by Sh (sometimes referred in the literature by θ or Y), and referred from now on as the Shields number.

The behavior of the C_D can be expressed as a function of the particle Reynolds number (Cliff et al. 1978). Some of those expressions, which are particle Reynolds number range dependent, are:

- for $0.01 \leq \mathrm{Re}_p \leq 20$:

$$C_D = \frac{24}{\mathrm{Re}_p}\left(1 + 0.1315\mathrm{Re}_p^{0.82-0.05\log\mathrm{Re}_p}\right) \tag{10}$$

- for $20 \leq \mathrm{Re}_p \leq 260$:

$$C_D = \frac{24}{\mathrm{Re}_p}\left(1 + 0.1935\mathrm{Re}_p^{0.6385}\right) \tag{11}$$

- for $260 \leq \mathrm{Re}_p \leq 1.5\times10^3$:

$$\log C_D = 1.6435 - 1.1242W + 0,1558W^2 \tag{12}$$

- for $1.5\times10^3 \leq \mathrm{Re}_p \leq 1.2\times10^4$:

$$\log C_D = -2.4571 + 2.5556W - 0.9295W^2 + 0,1049W^3 \tag{13}$$

with $W = \log \mathrm{Re}_p$.

Taking into account the referred expressions (10 to 13) for the C_D evaluation, equation (9) can be plotted and compared with the Shields diagram (correspondent to granular mixtures), considering the Reynolds number range variation (using $u_* \approx U_\infty/20$), and different support angles (Figure 4).

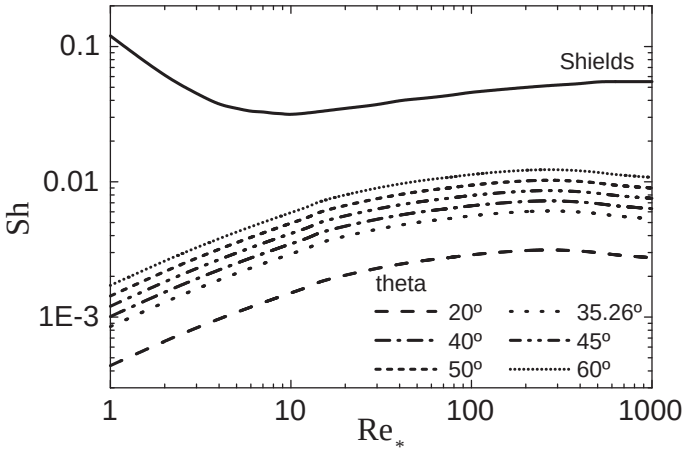

Figure 4: Comparison of Shields diagram with curves obtained for an isolated sphere, for different support angles (theta means θ).

For the turbulent regime, $\mathrm{Re}_* > 80$, and considering $\theta = 35.26^o$, the Shields number Sh, as calculated by equation (6) is approximately 0.006, which is about 10 times less than the value usual accepted for the Shields diagram in the same conditions, $Sh \approx 0.06$, (Cardoso 1998). In experiments carried out by (Fenton and Abbott 1977) a value of $Sh \approx 0.01$ was obtained, for large values of Re_*. Moreover, this last result is in good agreement with the ones obtained by (Coleman 1967).

In addition to the previous considerations one should also take into account the existence of turbulence forces, namely a turbulent drag and a turbulent

lift. Starting from the definition of drag force, and expressing the velocity in terms of a mean value and of a fluctuation component:

$$D = \frac{1}{2}\rho(u+u')^2 S C_D \tag{14}$$

or:

$$D = \frac{1}{2}\rho(u^2 + 2uu' + u'^2) S C_D \tag{15}$$

Applying the Reynolds average in order to eliminate the term uu' and taking into account the simplified theoretical hypothesis 3 referred before, one has:

$$\overline{D} = \frac{1}{2}\rho(U_\infty^2 + \overline{u'^2}) S C_D \tag{16}$$

expressing that the drag force has a contribution from the mean as well as from the fluctuating velocity components and it can be seen that the drag force has a contribution from the mean value of the flow and from the fluctuating component. A similar reasoning is valid for the lift force. It is then possible to individualize drag and lift turbulent forces, $\overline{D_t}$ and $\overline{L_t}$, with:

$$\overline{D_t} = \frac{1}{2}\rho\overline{u'^2} C_D S \tag{17}$$

$$\overline{L_t} = \frac{1}{2}\rho\overline{u'^2} C_L S \tag{18}$$

where u' = fluctuation of the longitudinal velocity.

Conducting a similar approach as before (neglecting the lift component), and again from the torque analysis equation (9) turns now into:

$$Sh = \frac{4}{3C_D}\tan\theta \frac{1}{U_\infty^{+2}}\left(\frac{1}{1+It_u^2}\right) \tag{19}$$

where $It_u^2 = \overline{u'^2}/U_\infty^2$, is defined as the turbulence intensity for the u component. If It_u is small compared with unity, equation (19) can be written as:

$$Sh = \frac{4}{3C_D}\tan\theta \frac{1}{U_\infty^{+2}}\left(1 - It_u^2\right) \tag{20}$$

The plot of this function is depicted in Figure 5 considering $\theta = 35.26^o$ for two different values of It_u. One can observe that the contribution of turbulence, although not relevant, shall be envisaged and taken into account, the most as more turbulent the flow is.

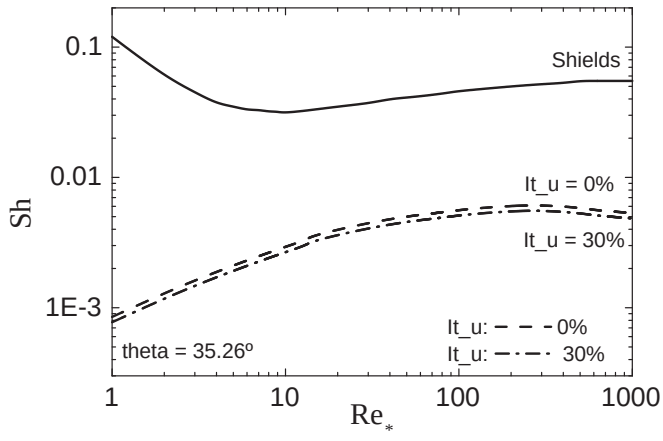

Figure 5: Variation of the Shields number with the turbulence intensity of the longitudinal velocity component (u) on the Shields number, for a support angle of $\theta = 35.26^o$ (It_u stands for It_u).

3 EXPERIMENTAL SETUP

The experiments were made on the flume channel of the Hydraulics Laboratory at FEUP. The channel is 0.4 m wide by 0.6 m high and has a length of 17 m.

On this channel a model similar to the one described before (Fig 1) was built in a *perspex* plate placed on the bottom of the water channel and the 5 mm diameter spherical particles used were made of glass ($\rho_s = 2.65\,\text{kgm}^{-3}$).

Table 1: Parameters of the LDV (m.c.v. stands for measurement control volume).

Parameter	Value	Comment
λ	514 nm	wavelength
θ	6.834º	angle of laser beams
δ_x	2.53 mm	major axis of m.c.v.
δ_y	162 μm	minor axis of m.c.v.
D_f	4.318 μm	fringe spacing
f_s	0.6 MHz	frequency shift

In order to measure the mean and turbulent velocities of the flow a one component laser Doppler velocimeter (LDV) system from DANTEC was used. The characteristics of this system are shown in Table 1.

The measurement grid used is depicted in Figure 6 and shows the plant view of the measured profiles.

4 EXPERIMENTAL RESULTS

In order to determine the conditions for the detachment of the test-particle (hereafter referred as critical conditions) several tests were carried out in order to obtain a narrow band of flow rate values for which the single test particle was removed, hereby referred

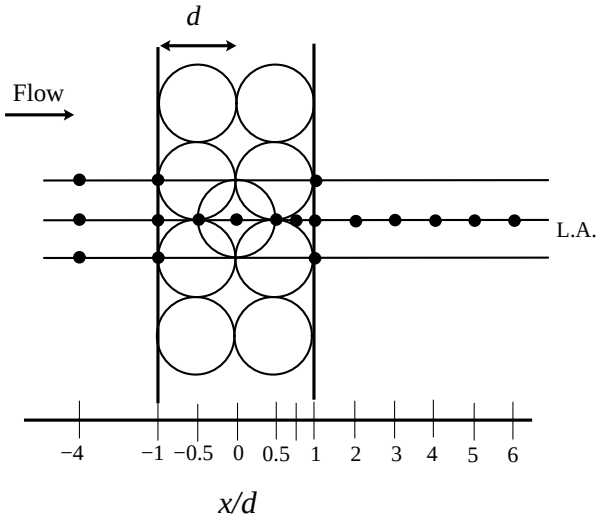

Figure 6: Top view of the measurement grid used in the measurements (L.A. stands for Longitudinal Axis).

as critical flow rate, Q_c. It was observed in the laboratory that the obtained interval for the critical flow rate was:

$$Q_c = [15.85;\ 17.25]\ \text{(L/s)} \tag{21}$$

The average flow rate obtained was 16.16 L/s and that was the flow value used as the critical flow case.

4.1 Studied flow characteristics

In order to allow the measurement for velocity fields characterisation in the critical condition to be made, the glass sphere was replaced by a steel sphere with the same diameter. The mean and turbulent velocity fields over and close to the test-particle were also characterised for two other flowrate values in the range below the critical one.

Table 2: Parameters of the flows considered

Re_h	Height h (m)	Q (L/s)	τ_w (Nm^{-2})
3.1×10^4	0.055	4.04	0.120
7.0×10^4	0.085	10.10	0.224
1.0×10^5	0.120	16.16	0.323

Table 4.1 summarizes the characteristics of the studied flows in terms of flow (Q), Reynolds number ($\text{Re}_h = UR_h/\nu$, where R_h is the hydraulic radius, U is the cross sectional mean velocity and ν is the kinematic viscosity) and shear stress (τ_w). The latter was evaluated by applying the Clauser method to the measured velocity profiles.

The flow fields characterization for any of those flows was carried for two situations: one with and the other without the test-particle placed in the flow. The last ones enabled the application of the Clauser's method. In fact, according to (Young 1989) from the log velocity law it is possible to demonstrate that the following relation holds:

$$\frac{u}{U_\infty} = \frac{1}{\kappa}\sqrt{\frac{C_f}{2}}\ln\left(\frac{U_\infty y}{\nu}\right) + \sqrt{\frac{C_f}{2}}\left(B + \frac{1}{2\kappa}\ln\left(\frac{C_f}{2}\right)\right) \tag{22}$$

where $C_f = 2\tau_w/\rho U_\infty^2$ is the skin-friction coefficient, $\kappa = 0.4$ is the von Kármán's constant and B is a constant. Choosing several values of C_f it is possible to determine a family of curves, and choose the one who better fits the obtained experimental data. In Figure 7 the Clauser method is illustrated for the critical condition, $\text{Re}_h = 1.0 \times 10^5$.

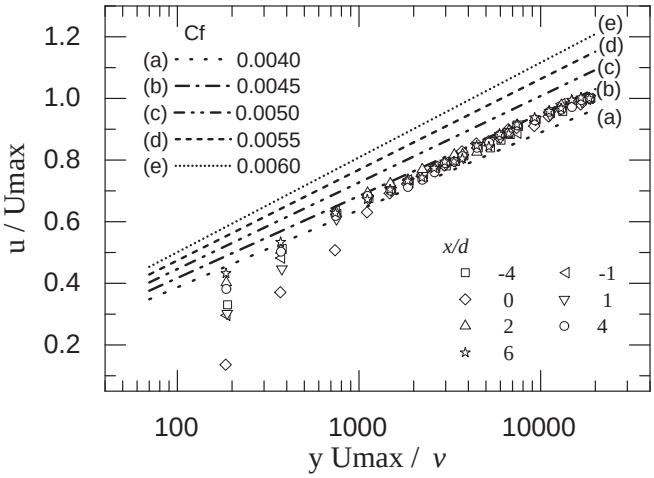

Figure 7: Application of the Clauser method to obtain the shear stress values on different longitudinal sections of the channel for $\text{Re}_h = 1.0 \times 10^5$ (take $U_{max} = U_\infty$).

As it can be seen the obtained values for C_f at different longitudinal sections, for the fitting range, are constant.

4.2 Analysis of the Conceptual Model

The conceptual model presented in the beginning of this paper is analyzed here in the light of the experiments. Using the flow characteristics (referred on Table 4.1), the correspondent Shields numbers (Sh) and Re_* could be obtained and are plotted in Figure 8 and listed on Table 3.

Comparing those values with the classical Shields diagram, also depicted on Figure 8, it is clear that, even for the determined critical condition, Shields' theory does not predict the beginning of particle motion. This is recognised to be due to the fact that the

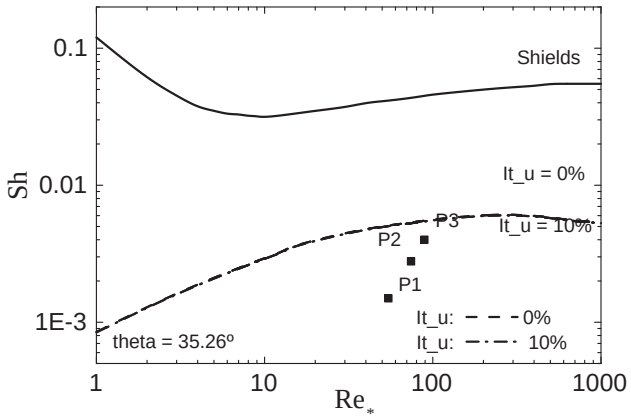

Figure 8: Comparison of the experimental results with the proposed conceptual model. Particle detachment situation corresponds to point P3 (obtained for the critical flow, $Re_h = 1.0 \times 10^5$). Points P1 and P2 correspond to the two other flows considered ($Re_h = 3.1 \times 10^4$ and $Re_h = 7.0 \times 10^4$, respectively).

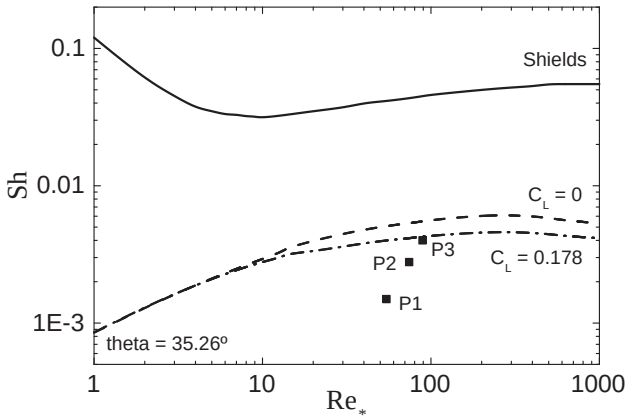

Figure 9: Comparison of the experimental results with the proposed conceptual model considering $C_L = 0$ and $C_L = 0.178$ as proposed by Einstein and Samni. Considering the lift coefficient the conceptual model gives results closer to the experimental ones.

Shields' criterion was derived considering the erosion of a granular bed of sediments and not only a single particle. Nevertheless the comparison is made since the Shields diagram is one of the important tools to assess the beginning of sediment motion and it is a very widely used reference for granular mixtures. It can be seen that (i) all the experimental points obtained present a consistent and crescent trend and (ii) the point correspondent to the critical flow (P3) is quite close to the line obtained by application of the simplified conceptual model, but still below the predicted critical value.

Table 3: Experimental data points obtained in the channel flume.

Point	Re_h	Re_*	Sh	Sh (Predicted)
P1	3.1×10^4	54	0.0015	—
P2	7.0×10^4	74	0.0028	—
P3	1.0×10^5	89	0.0040	0.0055

As referred before, the model assumes that there is no lift force contribution. It can be expected that if lift force is taken into account, the prediction of the critical value may be improved. In fact by considering the lift component, by adopting in equation (6) the value of $C_L = 0.178$ proposed by (Einstein and Samni, 1949), a new conceptual model curve may be obtained as depicted on Figure 9.

Figure 9 indicates that by considering the lift contribution the predicted critical values will be still in better agreement with experimental ones, and so the use of formulations for both C_L and C_D on the conceptual model is recommended.

4.3 Flow Field Over the Test-Particle

The use of the LDV, as referred, allowed to characterize mean velocity and turbulence intensity values on both longitudinal (u) and vertical (v) directions. Those measurements were carried out in the perspective of investigating the influence of the turbulence fluctuations and also the kinetic energy in the detachment process of the particle. Of course, that in addition of the characterization of the flow field for the critical condition case.

The velocity profiles corresponding to the critical condition ($\mathrm{Re}_h = 1.0 \times 10^5$) are depicted in Figures 10 to 13 and compare the behavior of the velocity field with and without test-particle along the longitudinal axis (see Fig 6).

Figure 10 shows that immediately upstream of the test-particle there is a reduction on the value of the longitudinal velocity (u) due to the deceleration of the flow. It is also clearly seen that over the test-particle there is an acceleration of the flow, with a high velocity gradient; on the other hand the wake region is characterized by a low velocity zone (with velocities about zero). The turbulence intensity (Fig 11) has a similar behavior but, in the wake region the higher values are located at a distance of the wall of about one diameter ($y/d \approx 1$). Over the test-particle turbulence intensity, It_u is about 18% (Fig 10).

For the v component, due to geometric limitations, it was not possible to make the measurements near the bottom. Nevertheless, it was possible to measure at a distance of $0.75\,\mathrm{mm}$ from the top of the sphere. The correspondent results are shown in Figures 12 and 13.

In terms of order of magnitude it can be concluded that the longitudinal mean component, u, is much

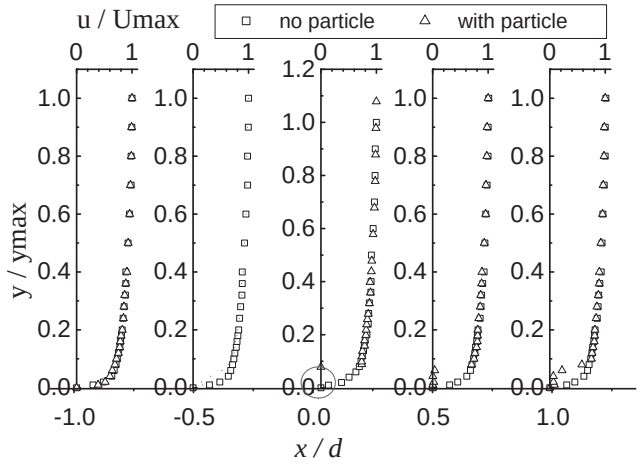

Figure 10: Mean velocity profiles of the u component on the test-particle for $\mathrm{Re}_h = 1.0 \times 10^5$, at the longitudinal axis (take $U_{max} = U_\infty$ and note that the circle is only to indicate the test particle height).

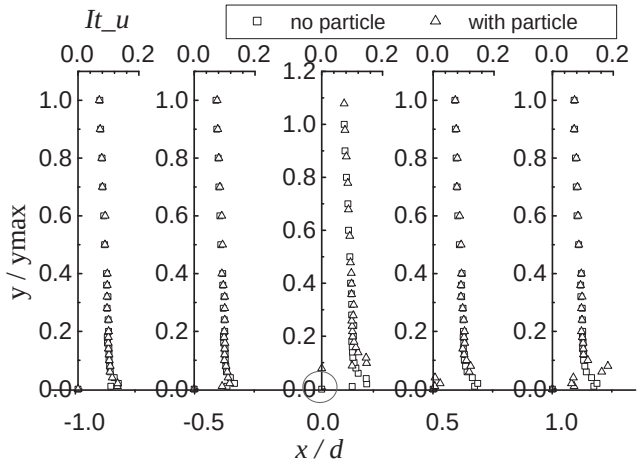

Figure 11: Turbulence intensity for the longitudinal component (u) over the test particle for $\mathrm{Re}_h = 1.0 \times 10^5$, at the longitudinal axis (take $U_{max} = U_\infty$, It_u = It_u and note that the circle is only to indicate the test particle height).

larger than the correspondent vertical component v. It is also possible to note that the turbulence intensity associated to the vertical velocity component (v) is of the same order of magnitude of the correspondent mean component.

4.4 Kinetic Energy Evaluation

Using the information available from the measured velocity profiles it is possible to determine the kinetic energy of the flow. In order to study the effect of the test-particle on the kinetic energy of the flow an analysis was made concerning sections $x/d = -1$ and

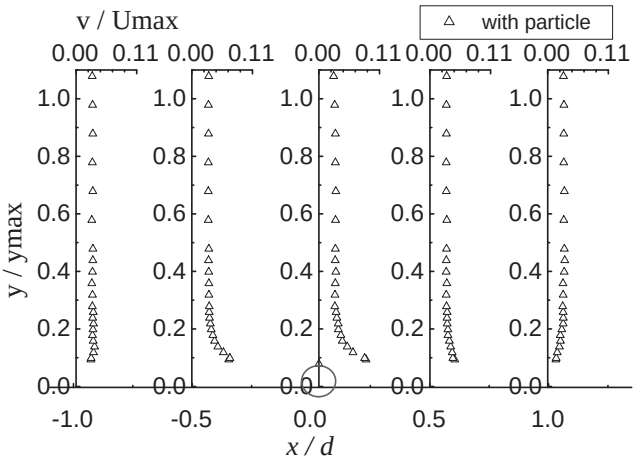

Figure 12: Velocity profiles of the mean v component on the test-particle for $\mathrm{Re}_h = 1.0 \times 10^5$, at the longitudinal axis (take $U_{max} = U_\infty$ and note that the circle is only to indicate the test particle height).

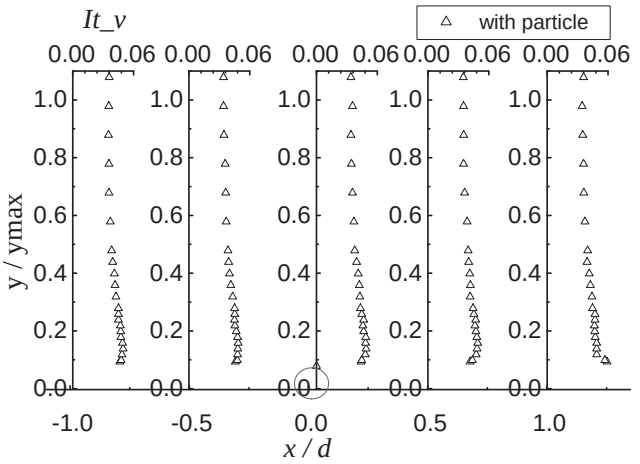

Figure 13: Turbulence intensity for the v component on the test particle for $\mathrm{Re}_h = 1.0 \times 10^5$, at the longitudinal axis (take $U_{max} = U_\infty$, It_v = $It_v = \overline{v'^2}/U_\infty$ and note that the circle is only to indicate the test particle height).

$x/d = +1$ (along the axis of the test-particle) by calculating the kinetic energy difference between those sections. The kinetic energy of the flow is given by (Hinze 1975):

$$k = \overline{k} + k' \tag{23}$$

where $\overline{k} = (\overline{u}^2 + \overline{v}^2 + \overline{w}^2)/2$ is the kinetic energy due to the mean components and $k' = (\overline{u'^2} + \overline{v'^2} + \overline{w'^2})/2$ is the kinetic due to the turbulent fluctuations of the flow. Due to experimental limitations the transverse

w component was not measured and so the following approximation was made:

$$k \approx \frac{1}{2}(\overline{u}^2 + \overline{u'^2} + \overline{v}^2 + \overline{v'^2}) \tag{24}$$

The difference between the kinetic energy of the flow measured at $x/d = +1$ and at $x/d = -1$ is then given by:

$$\Delta K = K_{+1} - K_{-1} \tag{25}$$

where K_{+1} = total kinetic energy at section $x/d = +1$; and K_{-1} = total kinetic energy at section $x/d = -1$. By dividing by u_*^2 equation (25) is made non-dimensional, which may be expressed by writing:

$$\Delta K^+ = K_{+1}^+ - K_{-1}^+ \tag{26}$$

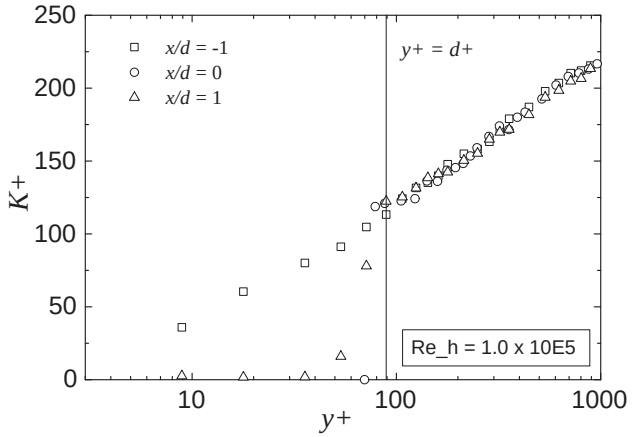

Figure 14: Total non-dimensional kinetic energy profiles measured at $x/d = -1$, 0, and $+1$ for the critical flow situation. Note that at $x/d = +1$ the total turbulent kinetic energy decreases significantly when compared with the one measured at $x/d = -1$.

Figure 14 shows the profiles of the total non-dimensional kinetic energy in $x/d = -1$, 0 and $+1$ for the critical flow situation ($\mathrm{Re}_h = 1.0 \times 10^5$) at the longitudinal axis.

The correspondent quantitative changes between the profiles at $x/d = -1$ and $x/d = 1$ are expressed in Figure 15.

In order to characterize the test-particle influence in the kinetic energy longitudinal variations it is possible to define the average kinetic energy between the

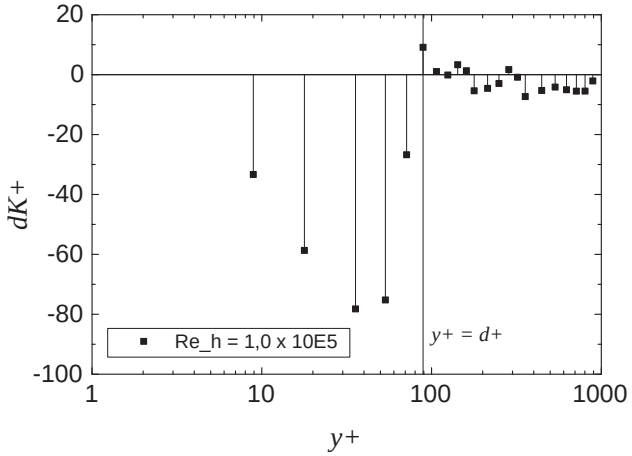

Figure 15: Total non-dimensional kinetic energy difference between profiles measured at x/d = -1 and $x/d = +1$ ($dK^+ = \Delta K^+$).

bed and the particle's top. This averaged value can be expressed in a non-dimensional form as:

$$\epsilon = \frac{1}{d^+}\int_0^{d^+} \Delta K^+ dy^+ \tag{27}$$

where $d^+ = u_* d/\nu$ is the non-dimensional height of the particle. ϵ may be interpreted as the mean value of the total kinetic energy difference between the bottom and d^+.

In dimensional form, the average value of the total kinetic energy difference may be expressed by:

$$e = \epsilon u_*^2 \tag{28}$$

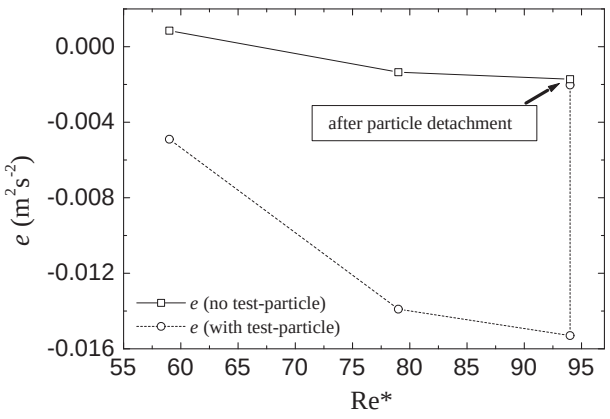

Figure 16: Variation of the e parameter with the shear Reynolds number considering two situations: with no test-particle and with test-particle. It can be seen that the test-particle acts as an energy dissipater.

On Figure 16 the variation of e is plotted against the variation of the shear Reynolds number Re_* for two cases: one considering the presence of the test-particle in the flow and other not considering it. From the case with test-particle it can be seen that the test-particle acts naturally as a kinetic energy dissipater, and it can be guessed that the particle will be detached if the flow has enough kinetic energy to remove it from its place. Further developments of this energy based method to assess the beginning of sediment motion are to be studied.

5 CONCLUSIONS

A conceptual model for the beginning of motion of a singular test-particle was presented that considers the influence of the drag and of turbulent drag forces.

The improvement of the model by considering the lift force contribution proved to enhance model accuracy, as should be expected. Although the complete form and adequacy of the conceptual model to the full range of shear Reynolds number has still to be validated, the obtained results of the model showed a good agreement with the ones obtained experimentally for the beginning of motion. In order to avoid approximations and use of inadequate data, the values of lift and drag coefficients should be calculated considering the particle Reynolds number and the shear rate $(\partial u/\partial y)$ near the wall.

It is known that turbulence is an important mechanism regarding the beginning of sediment motion. The presented model showed also that turbulence intensity contributed to influence particle detachment, but the formulation used, based on time averaged values, did not reveal that effect as mostly significant in current turbulent flows, as it could be expected. Improvements on this model should also be implemented in order to deal properly with the turbulence effects, namely by considering all velocity components, based on laser Doppler anemometry measurements.

Using the velocity profiles it was possible to study the flow field for the critical condition and estimate the kinetic energy of the flow (mean and fluctuation component). It is clear that the test-particle acts as a kinetic energy dissipater and that there is a threshold for which the test-particle is removed. That should be explored in order to better assess the beginning of particles motion.

6 ACKNOWLEDGMENTS

This work was supported by Fundação para a Ciência e Tecnologia grant, ref. POCTI/ECM/46693/2002.

The authors would also like to thank Professor Maria Fernanda Proença for the help in the LDV measurements.

REFERENCES

Cardoso, A. H. (1998). *Hidráulica Fluvial*. Lisboa: Fundação Calouste Gulbenkian.

Cliff, R., J. Grace, and M. Weber (1978). *Bubbles, Drops and Particles*. New York: Academic Press.

Coleman, N. (1967). A theoretical and experimental study of drag and lift forces actings on a sphere resting on a hypothetical stream bed. *Proc. 12th Congress, IAHR 3*, 185–192.

Fenton, J. and J. Abbott (1977). Initial movement of grains on a stream bed. *Proceedings of the Royal Society 352*, 523–537.

Goldstein, S. (1965). *Modern Developments in Fluid Dynamics vol.2*. New York: Dover Publications Inc.

Halliday, D., R. Resnick, and J. Walker (2001). *Fundamentals of Physics*. New York: John Wiley & Sons.

Hinze, J. O. (1975). *Turbulence*. New York: McGraw-Hill.

Nezu, I. and H. Nakagawa (1993). *Turbulence in Open-Channel Flows*. Rotterdam: A.A. Balkema.

Saffman, P. (1964). The lift on a small sphere in a slow shear flow. *Journal of Fluid Mechanics 22*(2), 385–400.

Shields, A. (1936). *Anwendung der Aenlichkeitsmechanik und der Turbulezforschung auf die Geschiebbewegung*. Ph. D. thesis, Mitteilungen der Preussischen Versuchsanstal fur Wasserbau und Schiffbau, Berlin.

Young, A. (1989). *Boundary Layers*. Oxford: BSP Professional Books.